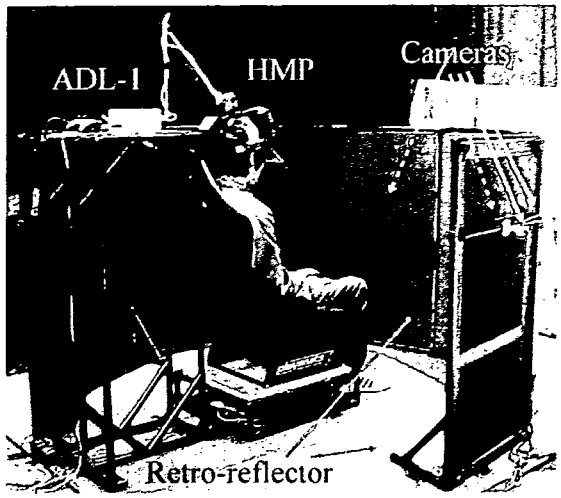

図 2: 装置の全体図

そこで概算の距離情報を高速に求めるため，元画像を縮小し，ノイズ除去のためガウシアンフィルタをかけ，さらにエピポーラ線を用いることでマッチングの高速化を図った．また画像全体の三次元座標を求めることは行わず，特徴的な点を初めに求め，その点の三次元座標を求めた．

1. カメラ A 中の特徴点を求める．
2. カメラ B とステレオマッチングを行い，特徴点の三次元位置を求める．
3. それらの特徴点の距離から，Virtual Screen の配置するべき奥行き距離を求める．

3. 装置

カメラは Point Grey Research 社製 FireflyMV(640×480) を用い，Head-Mounted Projector(HMP) は東芝 TDP-FF1A を元に自作した．カメラや再帰性反射材の配置は図 2 のようにし，ある物体が隣接する二つのカメラに同時に投影されるようにし，ほぼすべての領域でステレオマッチングによる距離を測定が可能となるようにした．

頭部には HMP と，位置計測装置 (Shooting Star Technology 社製 ADL-1) を取り付け，頭部の動きに合わせて HMP から映像を投影した．

4. 試作結果

実装したシステムを使用した結果，被写体の奥行き距離が取得できていることが確認できた．図 3 は実際に装置を用いて投影したときの映像を表しており，頭部の映像が観測位置から撮影した実映像，胸以下の部位については，外部カメラから取得した映像を再帰性反射材に投影した投影映像を表している．図 3 左の補正無しの状態では，Virtual Screen の奥行き距離が実際の被写体の奥行き距離とずれているため，実映像と投影映像の間のスケールがあっていない．しかし距離による補正をかけることで，図 3 右のように現実の映像と投影される映像が自然に接続されることが確認できた．

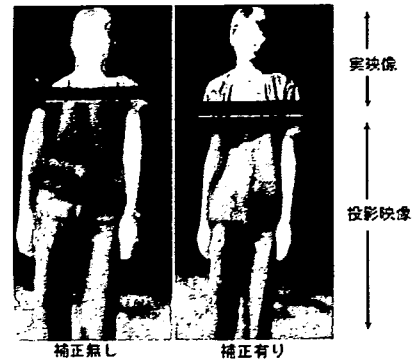

図 3: 未補正時に観測者が得られる映像 (左) と，補正をかけたときの映像 (右)

ただし，常に正しく補正されるわけではなく，補正をかけても画像にずれが生じる場合があることも判明した．

5. 考察

主にずれの原因となった要因は，ステレオマッチングの対応点の誤り，およびキャリブレーションの誤差があると推測される．

広い視野を得るために，カメラを離れて配置したため，二つのカメラで見える画像に差が大きく，マッチングが難しい．また，カメラの位置姿勢は手作業で合わせており，誤差を含んでいる．以上のような理由で，算出された距離にも誤差が含まれていたと推測される．

ステレオマッチングの対応点が正しい場合には，対象物体のほぼ同一の奥行き距離に Virtual Screen が配置され，実映像と投影映像の境界も自然に接続された．このような条件において，本手法は光学迷彩に於ける画像補正手法として有効に機能していることを示すことができた．

6. おわりに

提案した手法より，光学迷彩においてカメラを複数台用いて被写体の奥行き距離を動的に取得することで，被写体の動きにあわせた画像補正の可能性が示された．

今後は，今回課題となったステレオマッチングの精度向上や，カメラのキャリブレーションの問題などを解決し，システムの改良を進めていきたい．

参考文献

[1] M. Inami, N. Kawakami, D. Sekiguchi, Y. Yanagida, T. Maeda and S. Tachi: "Visuo-Haptic Display using Head-Mounted Projector", Proceedings of IEEE Virtual Reality 2000, pp.233–240,Mar.2000

[2] S. Tachi: "Augmented Telexistence", Mixed Reality-Merging Real and Virtual Worlds, pp.251–260, 1999

[3] M. Inami, N. Kawakami and S. Tachi: "Optical Camouflage Using Retro-reflective Projection Technology", Proceedings of the Second IEEE and ACM International Symposium on Mixed and Augmented Reality (ISMAR '03), 2003

Int J CARS (2007) 2:1–10
DOI 10.1007/s11548-007-0078-4

ORIGINAL ARTICLE

A real-time navigation system for laparoscopic surgery based on three-dimensional ultrasound using magneto-optic hybrid tracking configuration

Kozo Konishi · Masahiko Nakamoto · Yoshihiro Kakeji · Kazuo Tanoue · Hirofumi Kawanaka · Shohei Yamaguchi · Satoshi Ieiri · Yoshinobu Sato · Yoshihiko Maehara · Shinichi Tamura · Makoto Hashizume

Received: 13 November 2006 / Accepted: 6 March 2007 / Published online: 25 April 2007
© CARS 2007

Abstract
Objectives In laparoscopic liver surgery, intraoperative navigation is strongly recommended. We developed a navigation system based on intraoperative ultrasound (IOUS). The purpose of this study was to evaluate the usefulness and accuracy of this system using an animate model.
Materials and methods Augmented reality (AR) visualization superimposing three-dimensional ultrasound (3D-US) images onto captured laparoscopic live images was constructed. We employed magneto-optic hybrid tracking configuration and a rapid method of magnetic distortion correction. Twelve pigs and liver tumor mimics were used, and effects of magnetic distortion correction and accuracy of 3D-US navigation were evaluated.
Results Using magnetic distortion correction, tracking error was significantly reduced. Each ultrasound scanning time was within 30 s, and the time to generate 3D-US images was within 3 min. All tumor mimics were successfully puncture-guided with navigation. Registration accuracy was significantly improved from 17.2 ± 5.27 to 1.96 ± 0.87 mm.
Conclusion We developed an AR navigation system based on IOUS. Experimental results showed that the proposed method was effective, and could be used in clinical settings. 3D-US, as an imaging modality allows real-time imaging regardless of organ shifts or distortion.

Keywords Augmented reality (AR) · Navigation · 3D-US · Laparoscopic surgery · Image-guided surgery (IGS)

Abbreviations

IOUS	intraoperative ultrasound
AR	augmented reality
3D-US	three-dimensional ultrasound
DOF	degrees of freedom
ROI	region of interest
CT	computed tomography
RMS	root mean square
IGS	image-guided surgery

Introduction

The laparoscopic treatment of primary and metastatic liver tumors is feasible in appropriate settings [1–4]. However, indications of laparoscopic treatment are still limited despite

K. Konishi
Department of Innovative Medical Technology,
Kyushu University, Fukuoka, Japan

K. Konishi · Y. Kakeji · H. Kawanaka · S. Yamaguchi · Y. Maehara
Department of Surgery and Science,
Graduate School of Medical Sciences,
Kyushu University, Fukuoka, Japan

S. Yamaguchi · S. Ieiri · M. Hashizume
Department of Disaster and Emergency Medicine,
Graduate School of Medical Sciences,
Kyushu University, Fukuoka, Japan

K. Tanoue · M. Hashizume
Center for Integration of Advanced Medicine,
Life Science and Innovative Technology,
Kyushu University, Fukuoka, Japan

M. Nakamoto · Y. Sato · S. Tamura
Division of Interdisciplinary Image Analysis,
Osaka University Graduate School of Medicine, Osaka, Japan

M. Hashizume (✉)
3-1-1 Maidashi Higashi-ku, Fukuoka 812-8582, Japan
e-mail: mhashi@dem.med.kyushu-u.ac.jp

recent advances in laparoscopic techniques and instrumentations. One of the reasons may be the lack of intraoperative information such as tumor location, and relations to surrounding anatomical landmarks. In addition, limited views and lack of tactile sensation restrict the surgeon's abilities and stress the surgeon; therefore, additional information which could be used intraoperatively is strongly recommended.

Intraoperative ultrasound (IOUS) imaging is a useful and widely used intraoperative modality, especially in liver surgery because of its sensitivity in detecting liver tumors. IOUS has become the gold standard technique for detecting liver tumors, especially with the increasing numbers of lesions seen in patients who are typical candidates for radiofrequency ablation [5]. However, since ultrasound images have relatively low signal-to-noise ratio, are two dimensional, and offer a limited field of view, direct interpretation of the information from IOUS images remains difficult. Three-dimensional reconstructed imaging is useful to precisely simulate operative procedures, and could assist the surgeon in recognizing spatial relationships between tumors and surrounding tissues during laparoscopic surgery.

Recently, navigation systems have been widely used in various surgical fields, especially in neurosurgery, otorhinolaryngologic surgery, and spinal surgery [6–8]. Since laparoscopic surgery essentially involves monitor-based surgery, monitor-based augmented reality (AR) visualization can be naturally integrated into it. AR systems for microscopic neurosurgery based on preoperative 3D images have been reported [9,10]. However, in laparoscopic or thoracoscopic surgery, since the subject's organs are easily deformed or dislocated by surgical maneuvers and/or respiratory motions, AR visualization based on preoperative images have not yet been obtained.

In laparoscopic liver surgery, the main source of organ deformation is respiratory motion. Under general anesthesia, respiration is controllable, and endoscopic images can be acquired at the same respiratory phase as in 3D-US acquisition.

In order to acquire 3D-US data of the liver, the tip of a laparoscopic ultrasound probe should be tracked in the abdominal cavity. Although optical trackers are suitable for tracking rigid endoscopes with a rigid body attached outside the body, they are not appropriate for probe tip tracking due to line-of-sight constraints as the probe tip easily moves in the abdominal cavity to touch hepatic surfaces. On the other hand, magnetic trackers are particularly suitable for tracking within the abdomen. Therefore, we aimed to acquire 3D-US data using a magnetic tracker, and laparoscopic images were acquired by an optically tracked laparoscope.

However, the accuracy of magnetic trackers is greatly affected by magnetic field distortion resulting from metal objects and electronic equipments in close proximity, which is usually unavoidable in the operating room [11,12]. Therefore, the magnetic distortion correction is essential for accurate acquisition.

We previously developed a laparoscopic navigation system using the AR technology and a high-speed computer technology that generated three-dimensional images reconstructed from IOUS images and superimposed onto laparoscopic live images [13,14]. We recently developed and used a rapid method for magnetic tracker calibration using a magneto-optic hybrid tracking configuration.

The purpose of the present study was to clarify the effectiveness of this current navigation system and the accuracy of 3D-US reconstruction in animal experiments.

Materials and methods

Other papers have described our system design in details [13–16]. In the following sections, we provide a brief overview of our current system, and the full design of our current animal experiments for accuracy evaluation.

Augmented reality navigation system

System overview

Our navigation system consisted of a high-end ultrasound device SSD5500 (ALOKA, Japan) and a flexible US probe (ALOKA, Japan), an endoscope system (OTV-S5, Olympus, Japan), and a graphics and computing platform combined to the Virtual Place software (Medical Imaging Laboratory, Tokyo, Japan). We employed two different tracking systems: optical (Polaris, Northern Digital Inc., Canada) and magnetic (microBIRD, Ascension Technology Inc., USA) (Fig. 1).

The microBIRD system consists of a field generator, a control unit, and a miniature magnetic receiver. According to the official specification, position and orientation accuracy are 1.8 mm (RMS) and 0.5° RMS, respectively. Measurement volume is a sphere with a radius of 45.7 cm and center located at the magnetic field generator. The miniature magnetic receiver allows attachment of various tracked instruments which can be localized in the electromagnetic coordinate system in front of the field generator.

The Polaris system irradiates the object with ultra-red light and senses the light reflected from special reflection balls attached to the obeject. The official accuracy of polaris is 0.35 mm for single passive marker positioning and measurement volume is a sphere with a radius of 1.0 m and center located at 1.9 m from the camera.

The measurement rates of Polaris and miniBIRD were 30 and 120 fps according to their specifications, respectively. Both system can six degree-of-freedom tracking.

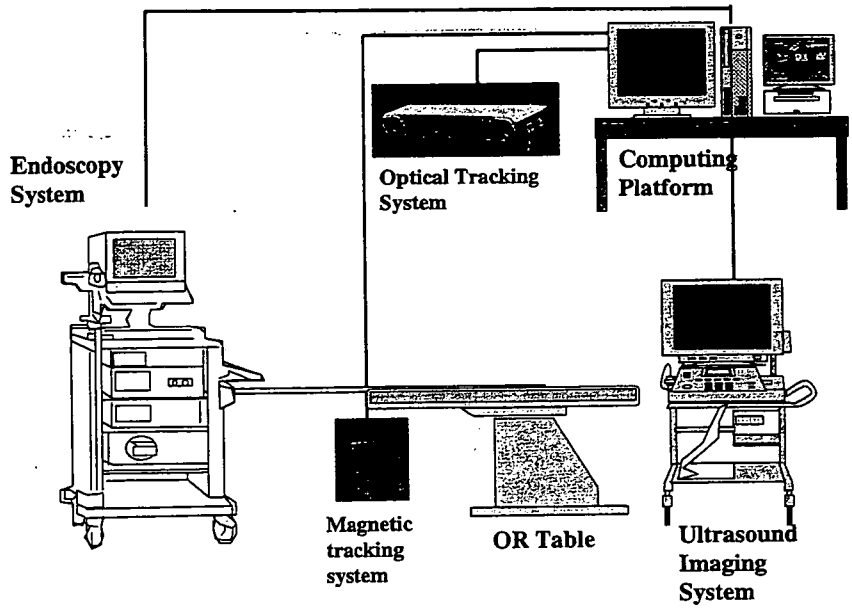

Fig. 1 System overview: schematic outline of the navigation system for endoscopic surgery. The 3D-US image is obtained in endoscopic surgery, and is superimposed on the endoscopic live images. Optical tracking system, magnetic tracking system, endoscopy system, and ultrasound imaging system are connected to computing platform

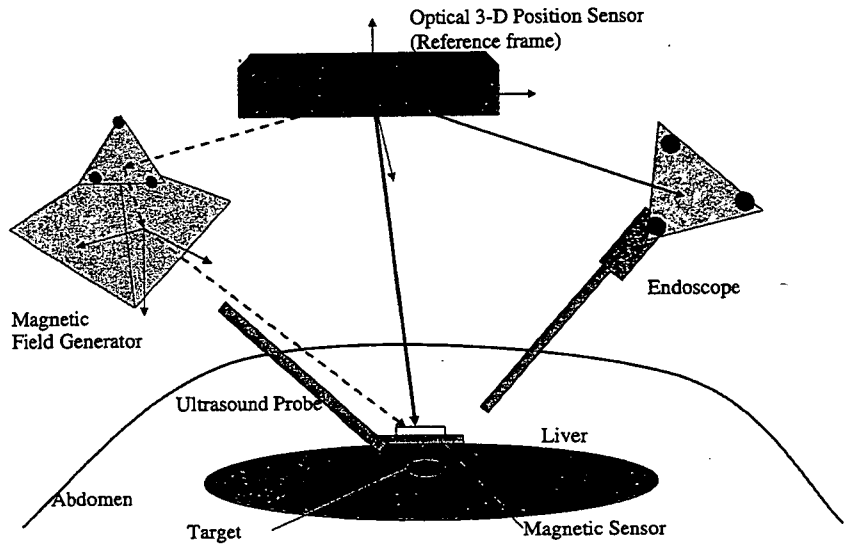

Fig. 2 System configuration: Relations among the coordinate systems involved in magneto-optic hybrid tracker. Endoscopic ultrasound probe, were magnetically tracked while rigid instruments such as rigid endoscopes were optically tracked. Optical position sensors were used as reference frame. A magnetic field generator and an endoscope were tracked by optical sensor. Ultrasound probe tip was tracked by magneto-optic hybrid tracking configuration

Intraoperative live video images from the ultrasound probe and the endoscope were digitized and fed into the *computing* platform (Fig. 1). The *computing* platform also received data on position and orientation of the ultrasound probe and the endoscope with magneto-optic hybrid tracking configuration described in [13] (Fig. 1). Figure 2 shows outline of the coordinate systems. For magneto-optic hybrid tracking, endoscopic instruments that could easily move inside the abdomen such as an endoscopic ultrasound probe were magnetically tracked while rigid instruments such as rigid endoscopes were optically tracked.

These data were adequately corrected and quickly combined in the computing platform. The generated 3D-US images were integrated into the endoscopic monitor, providing surgeons with AR visualization. In addition, using a computing platform, we performed plans based on preoperative CT, and we are now in the process of integrating these plans into intraoperative imaging.

3D-US navigation

Figure 3a shows setup for *endoscopic* 3D-US acquisition. A miniature magnetic receiver of the microBIRD system was attached to the ultrasound probe tip in order to obtain 3D position and orientation of the acquired US image planes. The probe tip moved in the abdominal or thoracic cavity to make full contact with the surface of the organ. The ultrasound calibration process is described in [11] in an environment without magnetic distortion.

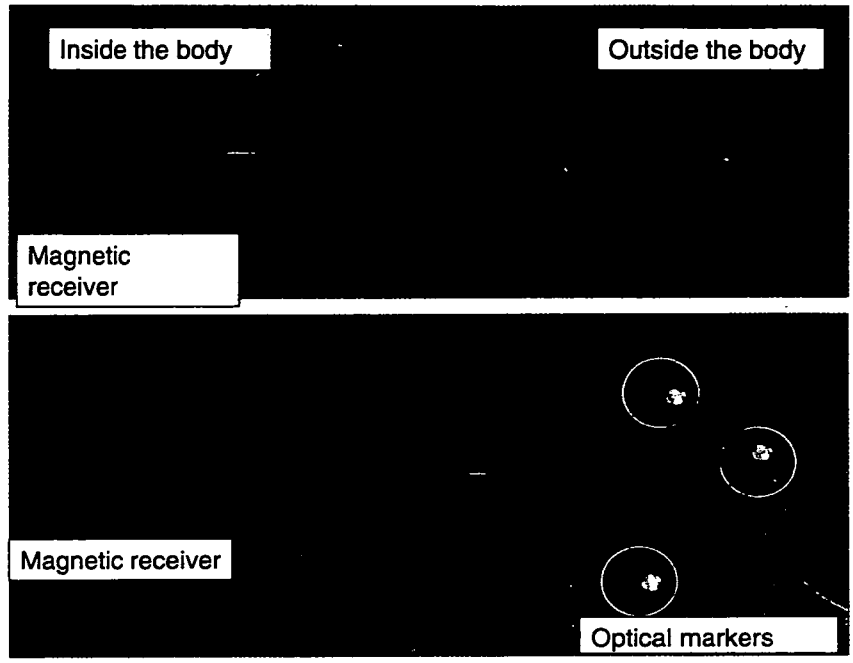

Fig. 3 Instruments for endoscopic ultrasound navigation. **a** Flexible ultrasound probe for endoscopic surgery (ALOKA, Japan). A magnetic receiver is attached to the tip of the probe. **b** Distortion measurement apparatus: a magnetic receiver and optical markers are attached

The procedure for reconstruction of 3D-US from ultrasound images has been described previously [12]. Briefly, in order to collect US images, a region of interest (ROI) was examined with a slow freehand sweep of the endoscopic probe at the end point of the expiratory phase. Data were stored on a workstation. Using coordinates of each single 2D image, 3D-US volume data reconstructions were generated based on the transformation equation [11,13] and visualized by a volume rendering method. We employed ray-casting method as volume rendering algorithm. 3D-US volume was rendered by perspective projection from the same viewpoint as the laparoscope, which was tracked by the Polaris system. Target constructions such as vessels or tumors were extracted by controlling opacity according to a histogram of the intensity of pixels in the target. Then, visualized 3D-US volume images were superimposed onto the captured endoscopic live images in accordance with 3D coordinates and AR visualization, and were displayed onto the monitor. The 3D-US images *followed* movements of the endoscope.

Calibration system of the oblique viewing endoscope

Advanced endoscopic surgeries including laparoscopic liver surgery require an oblique viewing endoscope because it is useful to secure a wide view while the camera head is fixed. An oblique viewing endoscope was designed so that the viewing direction could move by rotating a scope cylinder, even if the camera head was not moving. Although a camera calibration method is necessary to apply augmented reality technologies to oblique endoscopic procedures, no method for oblique scope calibration has been developed yet.

We previously developed a calibration system for an oblique viewing endoscope [16]. Briefly, a rigid body with optical markers was attached to the camera head for measuring its 6DOF pose parameters using an optical tracker, and the rotary encoder was geared to the scope cylinder for measuring its rotation parameters. Then, directions of laparoscopic views were calculated. We have evaluated the projection error of calibrated oblique viewing endoscope. The error was around 3 pixels [16].

Rapid calibration method for magnetic distortion correction

Electromagnetic trackers are significantly affected by magnetic field distortion resulting from metal and electronic equipments in the environment [14,15]. We demonstrated that the main strut of an operating table was the main source of magnetic field distortion [15].

In clinical settings for laparoscopic surgery, data sampling has to be performed just before 3D-US data acquisition, and should be done as rapidly as possible although the targeted space for distortion correction is small for 3D-US scanning. We proposed a rapid method for magnetic tracker calibration using a magneto-optic hybrid tracker [15]. Calibration data can be acquired by freehand using the distortion measurement apparatus with a hybrid tracker (Fig. 3b). An optical rigid body and a magnetic receiver are attached to this apparatus so that the position and orientation of the receiver can be simultaneously measured by optical and magnetic tracking methods.

To collect calibration data, a ROI where distortion correction is required was examined with a slow freehand sweep

of the measurement apparatus, twice at the end point of the expiratory phase.

One problem due to freehand data acquisition involves variable calibration accuracy resulting from changes in uniformity and density of the collected calibration data. To overcome this problem, we formulated a distortion model selection method using a cross-validation technique among five distortion models obtained by zeroth to fourth degree polynomial fitting to the calibration data [15]. The position accuracy of Polaris and microBIRD itself was 0.35 mm RMS and 1.4 mm RMS, respectively.

Design of the evaluation study

We performed animal experiments to clarify the clinical utility of the distortion correction method, as follows. Figure 3 shows the experimental environment for evaluation, where an electrically powered operating table (MIZUHO MOT - 5000) was used in order to simulate a clinical operative environment.

Twelve domestic pigs weighing 25–35 kg were used in the following experiments. Each pig was anesthetized and endotracheally intubated. All pigs were pharmacologically paralyzed using vecuronium (0.2 mg/kg). Ventilatory support and continuous monitoring of vital signs were performed.

All animals were treated under the protocols approved by the animal care committee of Kyushu University, and experiments were performed in accordance with both guidelines for Animal Experiments in Kyushu University, and the Law and Japanese notification.

Effects of magnetic distortion correction

We performed a comparative study of results of the receiver's orientation and angle on distortion correction using the correction procedure.

Data collection was performed laparoscopically by a freehand sweep with the measurement apparatus. The scanned space was located above the liver surface, and was approximately $10 \times 10 \times 2$ cm.

In addition, we evaluated the simplicity of the procedure and time required for magnetic distortion correction. It was thought that both these factors were important data in clinical cases.

Accuracy of 3D US navigation

In this experiment, laparoscopic surgical environment was simulated. Two pigs underwent laparoscopic procedures under general anesthesia and pneumoperitoneum.

Tumor mimics were made using a modification of the technique described by Nomori [17]. Briefly, a mixture of 8% purified agar and 25% gelatin dissolved in distilled water and 0.1% GD-DTPA was prepared. To maintain the mixture in a liquid form, it was kept at 80°C. Above 65°C, the mixture was liquid, was filled into syringes, and injected into livers using a 14G needle. Five agar injections were performed for two pigs each as nodular targets of approximately 2 cm in diameter. They became elastic hard tumors in the livers as temperature decreased.

After data were collected for distortion correction, US images of the tumor mimics were acquired, and 3D-US volumes were reconstructed using uncorrected and corrected magnetic 6D measurements for US probe tracking.

3D-US volume data reconstructions were generated and visualized by a volume rendering method. Tumors were extracted by controlling opacity. Then, visualized tumor images were superimposed onto the captured endoscopic live images in accordance with 3D coordinates.

AR navigation views were then constructed and displayed on the monitor. Needle punctures were performed while pigs were in the full expiratory phase. The needle was manually advanced toward a tumor in the liver under only AR navigation guidance. We utilized tumor depth information base on 2D ultrasound images and the needle scale.

The needle was advanced to a tumor to the shortest distance perpendicularly from the liver surface to reduce an error with the needle deformation.

We used an open configuration MRI detector (AIRIS II Hitachi Medical Company, Tokyo, Japan) for accuracy evaluation (Fig. 6).

At the final location of the needle insertion, needle position was then verified using MRI imaging. The axial MRI images in 3 mm thickness were collected for accuracy evaluation. We analyzed MRI images three dimensionally. To evaluate registration accuracy, root mean square (RMS) distances from the final needle tip position to the gravity center of the nodule were calculated in the 3D reconstructed volumes from MRI images.

When the puncture needle and the target tumor mimic were not well detected by MRI, we performed laparotomy, and directly measured positions of the tip of the puncture needle and the center of tumor mimics using a Polaris.

Data were reported as means ± SD. For statistical analysis, the Student t test was performed. A P value less than 0.05 was considered as a statistically significant difference.

Results

Effects of magnetic distortion correction

Magnetic distortion data for evaluation were sampled by the measurement apparatus successfully. Using magnetic distortion correction, error caused by magnetic distortion was significantly reduced from 34.64 ± 15.27 to 2.590 ± 0.913 mm

in position and from 9.077 ± 4.570° to 0.820 ± 0.782° in orientation (Fig. 4).

For freehand distortion correction, calculation time was less than 60 s, and data acquisition time was 67.8 ± 25.1 s. Number of the first data samples was 889.9 ± 431.2. Number of the second data samples was 861.1 ± 380.6.

Accuracy of 3D US navigation

Ultrasound images of tumor mimics were acquired, and 3D-US volumes were reconstructed using uncorrected and corrected magnetic 6D measurements with US probe tracking. AR images were successfully obtained (Fig. 5a–c).

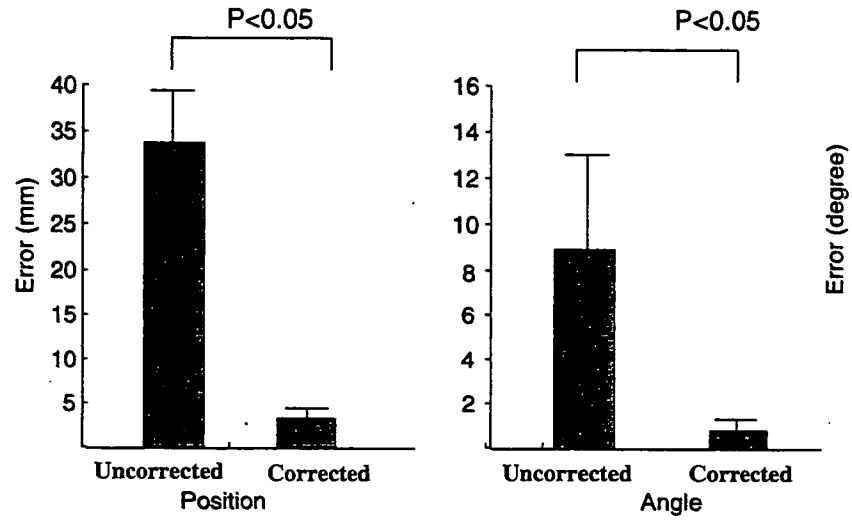

Fig. 4 Effects of rapid calibration for magnetic distortion correction. Using magnetic distortion correction, error caused by magnetic distortion was significantly reduced

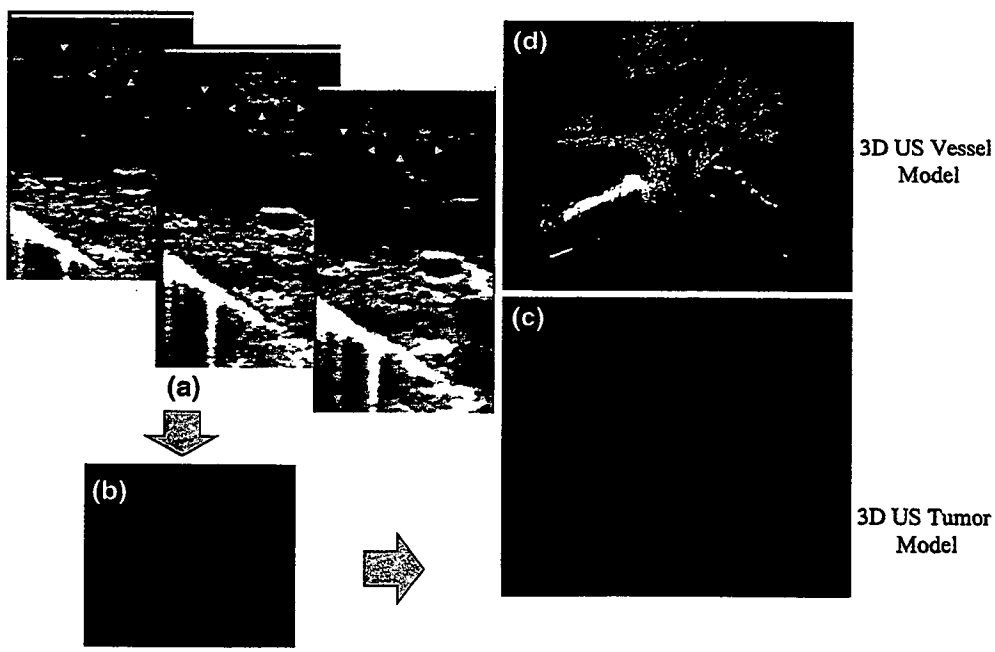

Fig. 5 The figures indicate obtaining a sequence of 2D ultrasound images of tumor (a), the volume- rendered 3D tumor image (b), and the 3D tumor image superimposed on the liver in laparoscopic images (c). The volume rendered 3D vessels extracted from color Doppler ultrasound images (d). a Two-dimensional ultrasound images of a tumor mimic. b Reconstructed from two-dimensional image data (a) and volume-rendered three-dimensional ultrasound image of a tumor mimic manually extracted according to the histogram. c Augmented reality image: three-dimensional tumor image (b) superimposed on to liver surface. d Augmented reality image: three-dimensional image reconstructed from Doppler ultrasound image of intrahepatic portal veins. Navigation can assist the surgeon in recognizing spatial relationships between tumors and vessels by superimposing 3D US data onto laparoscopic images

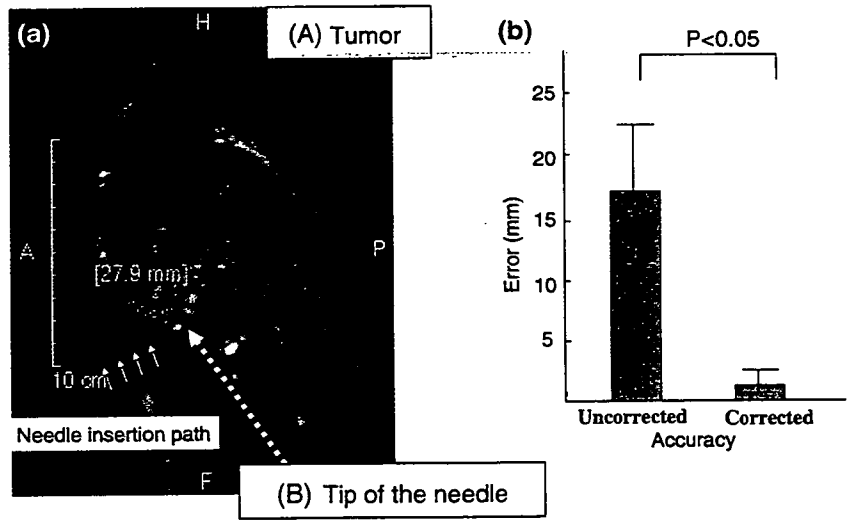

Fig. 6 Results of evaluation of magnetic distortion correction on AR navigation with MRI detector. **a** MRI image: A tumor mimic is visualized as high intensity tumor in T1 image (a *black dot arrow*), and puncture needle was visualized as low intensity (*white arrows*). The tip of the needle inserted with augmented reality navigation is also detected (a *white dot arrow*). **b** Effects of rapid calibration for magnetic distortion correction. Using magnetic distortion correction, accuracy of 3D-US navigation was significantly improved

Tumor mimics were visible as hyperechoic masses on ultrasound, and were easily segmented. Volume-rendered images of reconstructed 3D-US volumes of intra-hepatic portal veins were also overlaid onto the liver surface (Fig. 5d). Each ultrasound scanning time was within 30 s, and time loss due to distortion correction of the magnetic field and reconstruction of 3D-US images was within 3 min. As long as all positional information was measured correctly, our system operated normally, and 3D-US images were quickly updated and reconstructed, tracking real laparoscopic images. The update rate was approximately 5 Hz. All procedures were performed safely. Display latency due to lags in position measurements and rendering time requirements was so short that no operative procedures were disturbed.

All tumor mimics were depicted by high signals in T1 images from MRI, and the puncture needle was visualized as low signals (Fig. 6a). The measured size of tumor mimics was 6–14 mm in diameter. Using magnetic distortion correction, accuracy of 3D-US navigation was significantly improved from 17.2 ± 5.27 to 1.96 ± 0.87 mm RMS ($p < 0.05$) (Fig. 6b). All tumors were successfully punctured under the AR navigation guidance with magnetic distortion collection.

Discussion

The number of minimally invasive surgical approaches is increasing; especially, the indication of laparoscopic surgery for early cancer of abdominal organs has expanded. Laparoscopic surgery is a monitoring based surgery, i.e., a type of image-guided surgery (IGS), as almost all intraoperative information is integrated on a monitor. It is considered that techniques of IGS which have been introduced to other surgical fields may easily be applied to laparoscopic surgery. However, IGS using virtual reality technology for an abdominal region has not yet been used in the clinics. This might be due to two major problems including deformation of the liver and respiratory movements.

Due to large deformations and motions between preoperative images and intraoperative organs, non-rigid matching between these is required, making it difficult for clinical applications. Intraoperative imaging such as US imaging is an alternative way to avoid the difficulty of preoperative image matching [18,19].

Some kind of intraoperative imaging method such as 2D or 3D ultrasound imaging can be used to compensate for shifts in anatomy relative to preoperative CT/MR images. By using intraoperative 3D ultrasound, the surgeon can obtain updated anatomical images during a surgical procedure [18–20]. 3D-US as an imaging modality allows real-time imaging, regardless of organ shifts or distortions, and is available in every hospital.

We have developed a 3D-US system for laparoscopic surgery using a miniature magnetic tracker combined with an optical tracker to realize accurate tracking inside the abdomen, aiming at integrating a laparoscopic AR system. One potential drawback of magneto-optic hybridization is error propagation by combining two trackers. We confirmed by both simulations and laboratory experiments that error increased by magneto-optic hybridization was 0.1 or 0.2 mm for an appropriate rigid body size compared to a simple magnetic tracker [13,14].

In this paper, we demonstrated the accuracy and feasibility of a navigation system for laparoscopic surgery using animal experiments in the same environment as that in clinical settings.

Our results provide the basis for future clinical experiments. Clinical application of our navigation system for laparoscopic surgery relies on a rapid and reliable method. Our

system can provide calibrated data acquisition within 1 or 2 min. The whole procedure including distortion estimation and correction can be concluded within 5 min, which is within the permissible time period during operation.

Most of error derives from magnetic tracking and US scanning processes [22–24]. The rapidity of our method also enables on-the-spot validation because two calibration data sequences can be acquired from a region of interest within a short period of time. On-the-spot validation compensates for uncertainty of freehand data acquisition. Estimated accuracy by validation provides the surgeon with the criterion of distortion correction. If the estimated accuracy is not acceptable, the surgeon can repeat data acquisition or acquire additional data.

We consider that evaluation study with MRI was carried out as a pilot study that provided preliminary results. Actually, real-time imaging modality or needle tracking system is necessary to monitor the insertion of the needle. We did puncture with tumor depth information based on ultrasound images and the needle scale. Now, we are developing needle tracking system.

We think that the needle deformation is a big problem. To overcome this problem in the near future, we are now developing integrated navigation with real-time US or MRI.

Kleeman et al. [25] reported a laparoscopic navigation system based on IOUS. They also used an electromagnetic tracker to obtain 3D images, and concluded that further studies investigating accuracy and reproducibility in laparoscopic surgery were necessary.

We used experimental settings almost similar to those of the clinics, so our accurate experimental results revealed that our methods allowed minimally invasive treatment of liver tumors.

Distortion correction is an essential technology when using a magnetic tracker in endoscopic surgery, and it is thought that precision and data collection time are clinically significant factors with this technology.

Several clinical applications of navigation systems for bronchoscopy using magnetic tracking have been reported, and matching accuracy was 4.2–5.6 mm [26,27].

Accuracy of our navigation system was about 2 mm, and was superior to previously reported data. With about 2 mm of accuracy, superimposition of the 3D-US models of a small tumor or thin blood vessels is reliable. We consider that our results were attributed to the distortion correction effect. As for our methods of distortion, we could rapidly measure distortion of a magnetic field in the operative room, and adapt each environment to surgical fields. This was also an advantage, and confirmed the feasibility of our methods for clinical applications.

Furthermore, our system can be utilized with an oblique viewing endoscope, which is required in advanced endoscopic procedures. The superimposed virtual images tracked movements of laparoscopic views according to rotation of the camera head of the oblique viewing endoscope [14,28]. Therefore, our system is especially useful in advanced surgery.

The AR systems using 3D-US images have been developed for breast surgery to visualize tumors under the skin [11,12]. Assuming that organ deformation between 3D-US and endoscopic (or a video camera) image acquisitions is small enough, 3D-US images are regarded to match with endoscopic images without non-rigid registration.

On the other hand, 3D reconstructions from computed tomography (CT) and magnetic resonance imaging (MRI) can provide more sophisticated fine imaging, and can also be used for preoperative planning of complicated procedures. We previously established a "combined" AR navigation system which integrated preoperative CT/MRI images and IOUS images into the navigation software (Fig. 7), and have already applied that system to various clinical cases [28]. Three-dimensional reconstructions from CT and magnetic resonance imaging (MRI) can provide more sophisticated fine imaging, and can be used for preoperative planning of complicated procedures. CT is useful to especially visualize blood vessels compared to US. 3D-CT imaging provides details of the vascular system.

Our current matching approach makes use of landmarks based on direct methods to match the preoperative and endoscopic views together using the Polaris optical tracking system. With our system, simultaneous display of laparoscopic images and 3D-CT images can be obtained (Fig. 7).

Bao et al. [24] reported a US to CT registration method using an optically tracking US probe. The concept of their methods was almost the same as ours [24]. Since we cannot ignore shifts and deformations of an organ, it is difficult to obtain high precision that is necessary for a navigation system based on preoperative CT alone. However, CT imaging is advantageous when it is simultaneously used with ultrasonography. As for liver surgery, the surgeon can easily recognize spatial relationships between tumors and intrahepatic vessels using this combined technique. However, to establish useful IGS for liver surgery, an accurate registration method which superimposes images obtained from different modalities is required. If a complete IGS system could be devised for laparoscopic liver surgery, the number of candidates for laparoscopic treatment of liver tumors may increase [24,29,30]. Such an IGS system may also improve the quality of resection and local therapies such as radiofrequency ablation of liver tumors. We estimate that the IGS system may ultimately reduce recurrences and improve surgery.

While we first focused on liver surgery, our methodology can be applied to any other surgical fields. Currently, one of our targets is to apply our techniques to thoracoscopic surgery, especially for partial resection of small lung cancer. A more accurate navigation system is required in such cases,

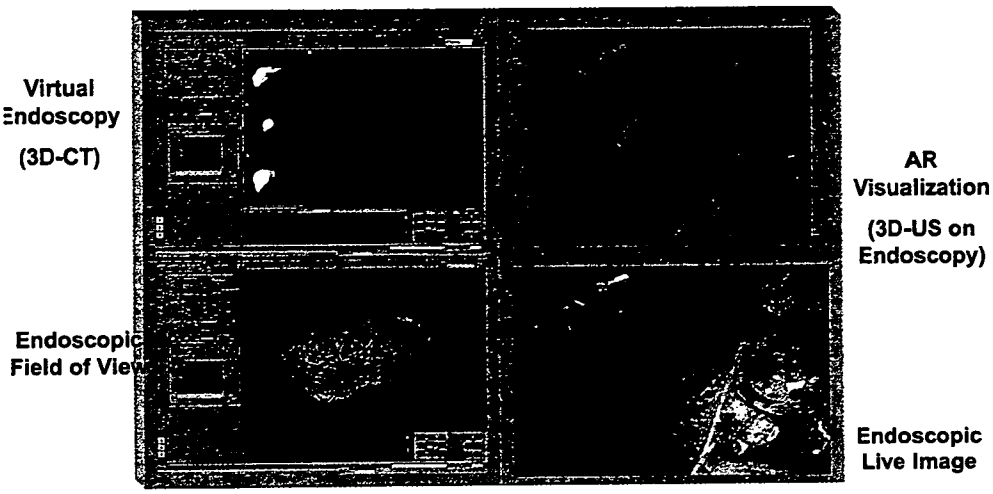

Fig. 7 Integrated display of navigation system based on 3D-CT and 3D-US with calibration system of oblique-viewing endoscope. *Upper left figure* shows structures in a liver constructed from preoperative CT images, and *upper right figure* represents AR visualization that presents a 3D ultrasound image overlaid on endoscopic view (*lower right figure*). *Lower left figure* represents a position and orientation of the current endoscopy with the liver

because when location of the tumor is not defined from the surface of the lungs, conversion to open surgery is required.

In the near future, we will attempt to increase accuracy of our present system, and develop a "clinically approved" multimodal matching method for capturing intraoperative organ deformations.

Conclusion

We developed an AR navigation system for laparoscopic liver surgery based on 3D-US. The system provides real-time anatomical information which cannot be otherwise visualized without navigation. Experimental results demonstrated that a rapid calibration method was effective, and is proposed to correct magnetic field distortion with an accuracy of 2 mm or less within 2 min. Therefore, 3D-US as an imaging modality allows real-time imaging, regardless of organ shifts or distortions. We believe that this navigation system will play a very important role in the future, and will contribute to improve safety of minimally invasive surgeries.

Acknowledgments This study was partly supported by the Research for the Future Program (JSPS-RFTF 99I00904).

References

1. Cherqui D, Husson E, Hammoud R, Malassagne B, Stephan F, Bensaid S, Rotman N et al (2000) Laparoscopic liver resections: a feasibility study in 30 patients. Ann Surg 232:753–762
2. Chung MH, Wood TF, Tsioulias GJ, Rose DM, Bilchik AJ (2001) Laparoscopic radiofrequency ablation of unresectable hepatic malignancies: a phase 2 trial. Surg Endosc 15: 1020–1026
3. Gigot JF, Glineur D, Santiago Azagra J, Goergen M, Camrick M, Morino M, Etienne J et al (2002) Laparoscopic liver resection for malignant liver tumors: preliminary results of a multicenter European study. Ann Surg 236: 90–97
4. Lesurtel M, Cherqui D, Laurent A, Tayar C, Fagniez PL (2003) Laparoscopic versus open left lateral hepatic lobectomy: a case–control study. J Am Coll Surg 196: 236–242
5. Wallace JR, Christians KK, Quiroz FA, Foley WD, Pitt HA, Quebbeman EJ (2001) Ablation of liver metastasis: is preoperative imaging sufficiently accurate. J Gastrointest Surg 5(1): 98–107
6. Hata N, Dohi T, Iseki H, Takakura K (1997) Development of a frameless and armless stereotactic neuronavigation system with ultrasonographic registration. Neurosurgery 41: 608–613
7. Cartellieri M, Kremser J, Vorbeck F (2001) Comparison of different 3D navigation systems by a clinical user. Eur Arch Otorhinolaryngol 258: 38–41
8. Gumprecht HK, Widenka DC, Lumenta CB (1999) BrainLab Vector Vision neuronavigation system: technology and clinical experiences in 131 cases. Neurosurgery 44: 97–105
9. Strong AJ, Chandler CL, Gleeson MJ (2000) Design and evaluation of a system for microscope-assisted guided interventions (MAGI). IEEE Trans Med Imaging 19(11): 1082–1093
10. Akatsuka Y, Kawamata T, Fujii M, Furuhashi Y, Saito A, Shibasaki T, Isaki H, Hori T (2000) AR navigation system for neurosurgery. In: Lecture notes in computer science, vol. 1935, Proceedings of the 3rd international conference on medical image computing and computer-assisted intervention (MICCAI 2000), Pittsburgh, PA, pp 833–838
11. Sato Y, Nakamoto M, Tamaki Y, Sasama T, Sakita I, Nakajima Y, Tamura S, Monden M (1998) Image guidance of breast cancer surgery using 3-D ultrasound images and augmented reality visualization. IEEE Trans Med Imaging 17(5): 681–693
12. Inoue T, Tamaki Y, Sato Y, Nakamoto M, Tamura S, Tanji Y, Taguchi T, Noguchi S (2005) Three-dimensional ultrasound imaging of breast cancer by a real-time intraoperative navigation system. Breast Cancer 12(2): 122–129
13. Nakamoto M, Sato Y et al (2000) Magneto-optic hybrid 3-D sensor for surgical navigation. In: Lecture notes in computer science (LNCS), vol 1935 (MICCAI 2000), pp 839–848
14. Nakamoto M, Sato Y, Miyamoto M et al. (2002) 3D ultrasound system using a magneto-optic hybrid tracker for augmented

reality visualization in laparoscopic liver surgery. In: Lecture notes in computer science(LNCS), vol. 2489 (MICCAI 2002), pp 148–155
15. Nakada K, Nakamoto M, Sato Y, Konishi K, Hashizume M, Tamura S (2003) A rapid method for magnetic tracker calibration using a magneto-optic hybrid tracker. In: Lecture notes on computer science, vol. 2879, Proceeding of MICCAI 2003, pp 285–293
16. Yamaguchi T, Nakamoto M, Sato Y, Konishi K, Hashizume M, Sugano N, Yoshikawa H, Tamura S (2004) Development of a camera model and calibration procedure for oblique-viewing endoscopes(dagger). Comput Aided Surg 9(5): 203–214
17. Nomori H (2005) Radiofrequency abation of pulmonary tumors and normal lung tissue in Swine and rabbits. Chest 127(3): 973–977
18. Hernes T, Ommedal S, Lie T, Lindseth F, Lango T, Unsgaard G (2002) Stereoscopic navigation-controlled display of preoperative MRI and intraoperative 3D ultrasound in planning and guidance of neurosurgery: new technology for minimally invasive image guided surgery approaches. Minim Invasive Neurosurg 46: 129–137
19. Kaspersen JH, Solie E, Wesche J, Åsland J, Lundbom J, Odegård A, Lindseth F, Hernes T (2003) 3D ultrasound based navigation combined with preoperative CT during abdominal interventions: a feasability study. Cardiovasc Intervent Radiol 26: 347–356
20. Harms J, Feussner H, Baumgartner M, Schneider A, Donhauser M, Wessels G (2001) Three-dimensional navigated laparoscopic ultrasonography: first experiences with a new minimally invasive diagnostic device. Surg Endosc 15(12): 1459–1462
21. Ellsmere J, Stoll J, Rattner D, Brooks D, Kane R, Wells W, Kikinis R, Vosburgh K (2003) A navigation system for augmenting laparoscopic ultrasound. In: Lecture notes in computer science, vol. 2879, Proceedings of the 6th international conference on medical image computing and computer-assisted intervention (MICCAI 2003), Montreal, Canada, pp 184–191
22. Birkfellner W, Watzinger F, Wanschitz F, Enislidis G, Killmann C, Rafolt D, Nowotny R, Ewers R, Bergmann H (1998) Systematic distortions in magnetic position digitizers. Med Phys 25(11): 2242–2248
23. Hummel JB, Bax MR, Figl ML, Kang Y, Calvin Maurer J, Birkfellner W, Bergmann H, Shahidi R (2005) Design and application of an assessment protocol for electromagnetic tracking systems. Med Phys 32(7): 2371–2379
24. Bao P, Warmath J, Galloway R, Herline A (2005) Ultrasound-to-computer-tomography registration for image-guided laparoscopic liver surgery. Surg Endosc 19(3): 424–429
25. Kleemann M, Hildebrand P, Birth M, Bruch HP (2006) Laparoscopic ultrasound navigation in liver surgery: technical aspects and accuracy. Surg Endosc 20(5):726–729. Epub 2006 March 16
26. Hautmann H, Schneider A, Pinkau T, Peltz F, Feussner H (2005) Electromagnetic catheter navigation during bronchoscopy: validation of a novel method by conventional fluoroscopy. Chest 128(1): 382–387
27. Turcza P, Duplaga M (2004) Navigation systems based on registration of endoscopic and CT-derived virtual images for bronchofiberoscopic procedures. Stud Health Technol Inform 105: 253–263
28. Konishi K, Nakamoto M, Miyamoto M, Hashizume M, Sato Y, Tamura S (2002) Development of AR navigation system for laparoscopic surgery using magneto-optic hybrid sensor: experiences with 3 cases. In: Proceedings of CARS2002, p 1093
29. Foroutani A, Garland AM, Berber E, String A, Engle K, Ryan TL, Pearl JM, Siperstein AE (2000) Laparoscopic ultrasound vs triphasic computed tomography for detecting liver tumors. Arch Surg 135(8): 933–938
30. Kane RA (2004) Intraoperative ultrasonography: history, current state of the art, and future directions. J Ultrasound Med 23(11): 1407–1420

原 著

低侵襲手術支援システムによる日本ー韓国間遠隔手術実験

A Remote Surgery Experiment between Japan-Korea using the Minimally Invasive Surgical System

荒田純平(正会員)[a*]，高橋弘樹(学生会員)[b]，割澤伸一(正会員)[b]，小西晃造(正会員)[c]，田上和夫(正会員)[c]，家入里志(正会員)[c]，清水周次[c]，中島直樹[d]，岡村耕二[e]，Young Soo KIM[f]，Sung Min KIM[f]，Joon-Soo HAHM[f]，橋爪誠(正会員)[c]，光石衛(正会員)[b]
[a]名古屋工業大学大学院工学研究科，[b]東京大学大学院工学系研究科，[c]九州大学大学院医学研究院，[d]九州大学病院，[e]九州大学大学院工学研究院，[f]漢陽大学医学部

Jumpei Arata[a*] , Hiroki Takahashi[b], Shin'ichi Warisawa[b], Kozo Konishi[c], Kazuo, Tanoue[c], Satoshi Ieiri[c], Shuji Shimizu[c], Naoki Nakashima[d], Koji Okamura[e], Young Soo Kim[f], Sung Min Kim[f], Joon-Soo Hahm[f], Makoto Hashizume[c], Mamoru Mitsuishi[b]
[a] Graduate School of Engineering, Nagoya Institute of Technology, [b] School of Engineering, The University of Tokyo, [c] Graduate School of Medical Sciences, Kyushu University, [d] Kyushu University Hospital, [e] Graduate School of Engineering, Kyushu University, [f] College of Medicine, Hanyang University

Abstract

In this paper, a remote surgery experiment, which was conducted between Japan and Korea by using the developed minimally surgical system is described. A research Internet, APII (Asia-Pacific Information Infrastructure), which consists of an optical submarine cable network, KJCN (Korea-Japan Cable Network) was used as an information transmission channel. In the experiment, a laparoscopic cholecystectomy was successfully performed on a pig. The network time-delays of robot and images were 6.5 ms and 435 ms respectively.

Key words

Remote surgery, Surgical robot and Minimally invasive surgical system.

1. はじめに

遠隔手術の実現は，優れた医師の遠隔地からの手術参加を可能とし，また過疎地，極限環境等における手術実現，さらに国境を越えたチームワーク医療を容易に実現することが可能となり，加えて優れた医療技術を世界へ普及させるための教育効果が期待できる．本研究では，遠隔手術実現のため，低侵襲手術支援システム[14]を開発し，これまで4回にわたり東京ー静岡(直線距離約 150km)を結ぶブタを対象とした腹腔鏡下胆嚢摘出術手術実験を行なった．遠隔手術を行なう際，通信手段として専用線を用いることにより安定した通信品質を得ることが可能である．しかし将来的に遠隔手術が広範に適用されるためには，専用回線を用いる

*名古屋工業大学大学院工学研究科つくり領域
〒466-8555 名古屋市昭和区御器所町
jumpei@nitech.ac.jp
受付 2006 年 7 月 26 日；採択 2006 年 11 月 10 日

より高度に普及が進んでいるインターネット回線を用いることが望ましい．よって，これらの遠隔手術実験においては既存の情報通信設備を使用することを想定し，国内の病院等施設に広く普及しているISDN(2B+D), ISDN (23B+D)回線を用いた．ロボット制御信号の伝送時間遅れは 50ms，また映像伝送時間遅れは 400ms程度であり，いずれの手術も成功することが可能であった．手術に要した時間は 1 時間程度であり，ほぼ従来の手術と変わらなかった．

そこで本研究では，さらに広範に遠隔手術が普及するための通信手段として，インターネットを用いた遠隔手術実現における知見を得るため，日本ー韓国間において学術研究用インターネットを用いた遠隔手術実験を行なった．本実験では日本ー韓国間を結ぶ回線として，福岡と釜山を結ぶ光海底ケーブルKJCN (Korea-Japan Cable Network)で構成された，日韓インターネット・テストベッドAPII (Asia-Pacific Information Infrastructure)[17]を使用した．APIIの両端は，それぞれインターネットと接続された大学内LAN等，一般ユーザが利用するネットワークを介している．

2. 関連研究

現在，多くの手術ロボット開発が行なわれており，その多くは内視鏡等を用いて患者体内で複雑な動作を実現することで医師を支援し，より低侵襲な手術を実現することを目的としている．Salisbury らは先端部にワイヤ駆動方式を用いた手術ロボットシステムda Vinci[1]を開発し，多くの臨床結果が報告されている．Taylorらは力帰還制御を応用したマイクロサージェリシステムを開発した[2]．生田らはワイヤ駆動を用い，先端に多自由度を有する手術ロボットを開発した[3]．佐久間らは内視鏡保持ロボット，また低侵襲腹部外科支援ロボット等を開発した[4]．藤江らは4自由度を有する脳外科用マイクロサージェリシステムを開発した[5]．

筆者らは，低侵襲手術支援システムを開発し，特に操作器(マスタ)と手術ロボット(スレーブ)を遠隔に配置し，手術を行なう遠隔手術についての研究を行なっている[14)-16)]．遠隔手術の研究として，Greenらは各5 自由度の左右腕を有するマスタ・スレーブ型ロボットを開発し，縫合実験を行なっている[6]．このシステムはその後，上記da Vinciとして発展した．新井らは血管内に挿入するカテーテルを高速ネットワークを用いて遠隔操作を行なうシステムを開発した[7]．Rovettaらは ISDN回線を用いた遠隔手術の研究を行なった[8]．Salcudeanらはサイズ効果を考慮した遠隔操作についての研究を報告している[9]．Marescauxらは専用ATM回線を用い，手術ロボットZEUSによるNew York－Strasbourg間遠隔手術を実施した[10]．

3. 低侵襲手術支援システム

低侵襲手術支援システムは，2 つのサイト(場所)により構成される．オペレーション・サイトは，執刀医が存在し，操作を行なう場所であり，また，サージェリ・サイトは，患者が存在し，実際の手術が行なわれる場所である．これらの 2 つのサイトは LAN による接続，または ATM，ISDN 等，様々な回線種別により接続可

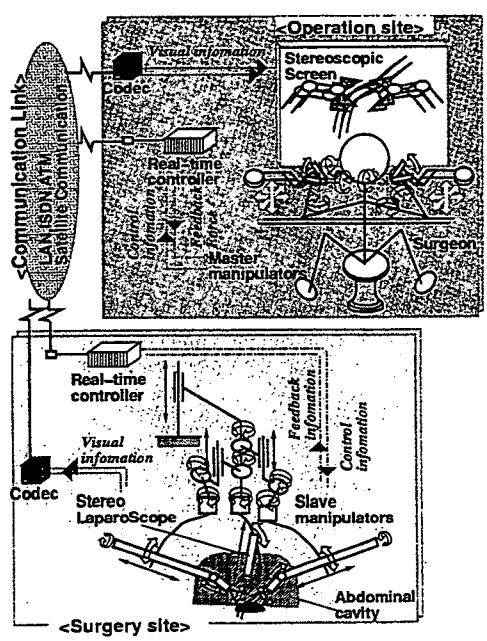

Fig.1 Overview of the developed system.

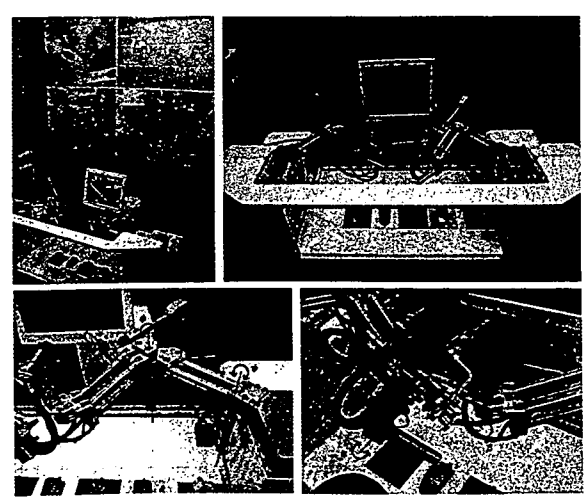

Fig.2 Master manipulator.

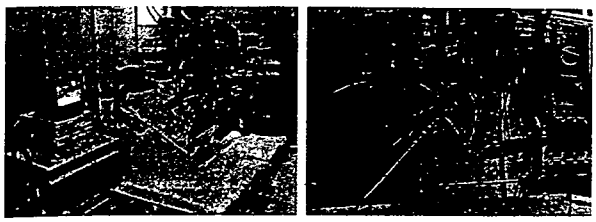

Fig.3 Slave manipulator.

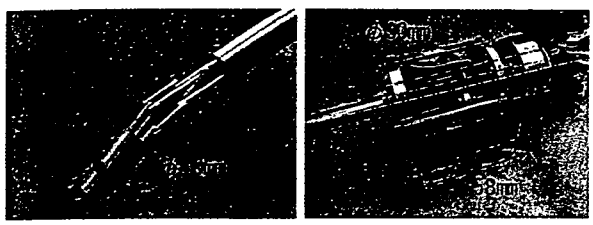

Fig.4 Link driven multiple DOF forceps.

能であり，ロボット制御信号，映像，音声等が伝送される(Fig.1)．マスタ・マニピュレータ，スレーブ・マニピュレータは VxWorks を用いて実時間制御され，制御周波数を 1kHz としている．マスタ・スレーブ間制御信号の通信周波数は相互を結ぶ通信帯域により変更可能であり，今回の遠隔手術実験では 10Hz とした．

オペレーション・サイト：手術の執刀を行なう医師はオペレーション・サイトにおいて，操作入力器であるマスタ・マニピュレータにより動作入力を行なう．医師によって入力された操作情報は，リアルタイム・コントローラによって絶対位置情報への変換のため，幾何学計算が行なわれた後，制御信号として情報伝送システムを介してサージェリ・サイトへ伝送される．マスタ・マニピュレータは左右 2 腕から構成され，片腕につき並進 3 自由度，姿勢 3 自由度，開閉 1 自由度の計 7 自由度を有する(Fig.2)．並進動作させたとき，先端部姿勢が変化しないリンク機構を有し，実時間制御における計算量を機構面から減少させている．

サージェリ・サイト：サージェリ・サイトでは，オペレーション・サイトより伝送された制御信号をもとに，スレーブ・マニピュレータが動作することにより手術が行なわれる．このときの内視鏡映像，またその他バイタルサイン，術場フィールド映像等の環境情報は同じくオペレーション・サイトへ伝送され，執刀医へ提示される．同様にオペレーション・サイトの操作者の映像・音声はサージェリ・サイトへ伝送され，サージェリ・サイトの助手への指示等に使用される．スレーブ・マニピュレータは，内視鏡用アーム 1 腕，手術ツール用アーム 2 腕の計 3 腕から構成され，各アームは曲率ガイドを用いた機構的不動点を中心とする回転 2 自由度，長軸方向の並進 1 自由度を有する(Fig.3)．この構造により患者の安全性を機構的に保証することが可能である．手術ツール用アームは，ポート刺入位置決定のための機構部全体を並進させる 3 自由度を有する．また，3 腕全体を鉛直方向に並進させる 1 自由度を有する．手術ツールとして，電気メス等の既存製品，リンク駆動式多自由度屈曲鉗子等が取り付け可能である．リンク駆動式多自由度屈曲鉗子の外径は 10mm であり，先端部で屈曲 2 自由度，開閉 1 自由度を有する(Fig.4)．これらの鉗子先端自由度は，リンク機構によって生成され，ワイヤ駆動方式と比較して，伸び，切断等の問題がなく，滅菌・洗浄性に優れ，メンテナンスが容易な特徴がある．

Table 1 Surgical procedures of laparoscopic cholecystectomy.

No.	Surgical procedure
1	Insertion of surgical instruments (setup)
2	Creating working space by moving organs
3	Exfoliation cystic duct and arteria cystica
4	Treatment of cystic duct and arteria cystica
5	Resection of cholecyst
6	Extraction of cholecyst

4. 日本－韓国間遠隔手術実験

4.1 実験目的

本研究ではこれまで，既存の情報通信設備として ISDN 回線を使用した遠隔手術実験を行なった．さらに本実験では，日本－韓国を結ぶ学術研究用インターネット APII を介して低侵襲手術支援システムにより手術を行ない，情報伝送により生ずる伝送時間遅れの影響を調べた．これにより，これまでの ISDN を用い

Fig.5 Aspect of the operation site (Hanyang Univ.).

Fig.6 Aspect of the surgery site (Kyushu Univ.).

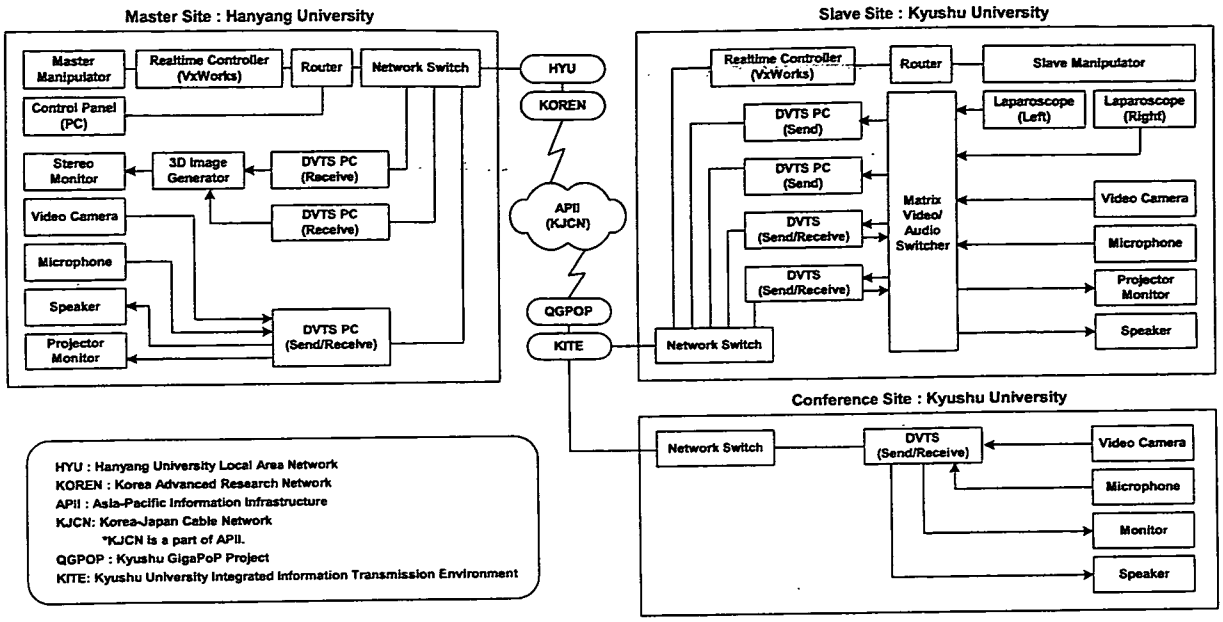

Fig.7 Overview of the network configuration.

た実験での伝送時間遅れの影響等の比較検証を行ない，遠隔手術実現のための知見を得ることが本実験の目的である．

4.2 実験方法

本実験では，下記の実験システム構成のもと，低侵襲手術支援システムによるブタを対象とした腹腔鏡下胆嚢摘出術を行なった．本研究は九州大学大学院医学研究院附属動物実験施設の承認を受けた上で規約を遵守し，動物実験に関する教育訓練を受けた医師により実施された．

腹腔鏡下胆嚢摘出術：腹腔鏡下胆嚢摘出術とは，腹腔鏡，および患者腹腔内に手術器具を挿入し胆嚢を摘出する手術方法である．その主な手順を **Table 1** に示す．

実験施設：実験施設として，オペレーション・サイトを漢陽大学(17 Haengdang-dong, Seongdong-gu, Seoul, **Fig.5**)，またサージェリ・サイトを九州大学(福岡市東区馬出 34-1, **Fig.6**)として実験を行なった．両サイト間の直線距離は約 540km である．九州大学では，カンファレンス・サイトが設けられ，術中，日本・韓国の参加医師らによるディスカッションが行なわれた．

実験システム構成：本実験で用いたネットワーク回線構成を **Fig.7** に示す．ネットワーク伝送経路は，九州大学から学内 LAN (KITE: Kyushu University Integrated Information Transmission Environment)を経由し，日本ー韓国を結ぶギガビットクラス幹線である APII テストベッドを介し，韓国の学術ネットワークである KOREN (Korea Advanced Research Network)へ乗り入れ，漢陽大学内 LAN へ接続される．

ロボット動作情報においては，TCP/IP ネイティブ・ソケットによる通信を確立した．低侵襲手術支援システムのマスタ・スレーブ間の通信はマスタ側リアルタ

Table 3 Time-consuming chart of surgical procedures (including the discussion during surgical procedures).

Time	Precedure
0:00	Inserting trocars
0:15	Inserting a laparoscope
0:30	Inserting the robotic forceps
0:55	Finishing the surgical setup
0:57	Starting the remote surgery
1:20	Switching right forceps to an radio knife
1:30	Cutting a cholecyst
2:33	Cutting a cystic duct
2:47	Finishing cutting a cholecyst
3:00	Operation completed

Table 2 DVTS data transfer bandwidth.

Image	Bandwidth
From surgery site to operation site:	
Conference Use	15Mbps
Laparoscope (Right)	10Mbps
Laparoscope (Left)	10Mbps
From operation site to surgery site:	
Conference Use	15Mbps
Total	50Mbps

Table 4 Network time-delay by ping (Round-trip).

Network	Used bandwidth	Op. site – Surg. site	Distance	Hop	Time-delay
ISDN(2B+D)	128 Kbps	Tokyo - Shizuoka	150 km	-	99.8 ms
ISDN(23B+D)	1472 Kbps	Tokyo - Shizuoka	150 km	-	35.6 ms
APII	50 Mbps	Seoul - Fukuoka	540 km	14	13.0 ms

Table 5 Image time-delay (Round-trip).

Network	Used bandwidth	Op. site – Surg. site	Distance	CODEC	Time-delay
ISDN(2B+D)×2	256 Kbps	Tokyo - Shizuoka	150 km	SONY PCS-P500	676.0 ms
ISDN(23B+D)	1472 Kbps	Tokyo - Shizuoka	150 km	NEC TC5000EX100	785.0 ms
APII	50 Mbps	Seoul - Fukuoka	540 km	DVTS	871.0 ms

イム・コントローラより，10Hzの周期で制御信号がスレーブ側リアルタイム・コントローラへ送信された．本実験で用いた映像・音声伝送手法はDVTS(Digital Video Transfer System)であり，DV品質を非圧縮で伝送するものである．DVTSはWIDEプロジェクト[18]ほかで研究開発が進められており，ハードウェア・タイプとソフトウェア・タイプが存在する．本実験では，九州大学側では両方のタイプを，漢陽大学側ではソフトウェア・タイプを使用した．DVTSによる映像伝送は，通常 1 系統の送信につき約 30Mbpsの帯域を使用するが，フレームレートを変更することにより使用帯域を低減することが可能である．漢陽大学－九州大学間においては，**Table 2** に示すように，全4系統，合計50Mbpsの映像が送受信された．本実験では，伝送フレームレートをカンファレス用映像 15fps，内視鏡映像 10fpsと設定した．また内視鏡映像伝送として，新興光器製作所社製三次元立体視腹腔鏡を低侵襲手術支援システムへ組み込み，左右眼それぞれの映像を伝送し，オペレーション・サイトにおいて三次元映像として合成した後，操作者へ提示した[16]．

4.3 実験結果と考察

低侵襲手術支援システムを用い，日本－韓国を結ぶ学術研究用インターネットを介したブタを対象とした腹腔鏡下胆嚢摘出術を行なうことに成功した．実際の手術に要した時間は約 1 時間程度であり，従来の手術手法，これまでに行なった遠隔手術実験とほぼ変わらない結果であった(**Table 3**)．

伝送時間遅れ：伝送時間遅れを調べるため，その指標として ping による Round-trip time の測定を行なった(**Fig.8**)．本実験におけるネットワーク環境において，低侵襲手術支援システムで使用したパケット・サイズ 144byte での Round-trip time は，13ms であった．このことから，マスタ・スレーブ間における制御信号は約 6.5ms で到達していたと考えられる．これまでの東京－静岡間の ISDN を使用した実験と比較して，大きく向上していることが確認された(**Table 4**)．映像伝送について，ストップ・ウォッチ映像をループバックさせることにより，測定伝送時間遅れを測定した．サージェリ・サイトからオペレーション・サイトへ伝送される 3 系統の映像のうち，内視鏡映像に用いられた 1 系統について測定を行なった．10 フレームについて測定し，その平均値を求めたところ，Round-trip で 871.0ms であった(**Table 5**)．東京－静岡間の ISDN(2B+D)2 回線，ISDN(23B+D)を用いた実験では CODEC として，それぞれ SONY PCS-P500，NEC TC5000EX100 を用いた．これらの結果は使用したネットワーク構成，CODEC，伝送した映像系統数等，条件が大きく異なるため，一元的な比較はできないが，本実験では過去の実験と比較して倍に当たる 4 系統の映像を伝送したにもかかわらず，これまでの実験とほぼ同程度の伝送時間遅れで伝送可能であった．映像品質においては，本実験で用いた DVTS は，DV 品質を非圧縮で伝送することから，大幅に向上した．なお，本実験では内視鏡映像を 10fps で伝送を行なったが，術者の操作感においては 15fps での伝送と比較しても違いは得られなかった．

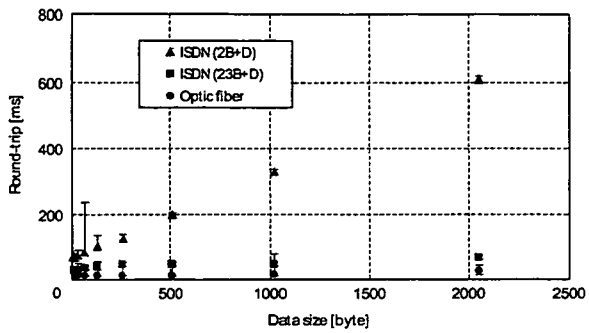

Fig.8 Network time-delay comparison by ping.

操作者が体感する時間遅れは，これらの伝送時間遅れをもとに，マスタ・スレーブ間の送信周期，位置情

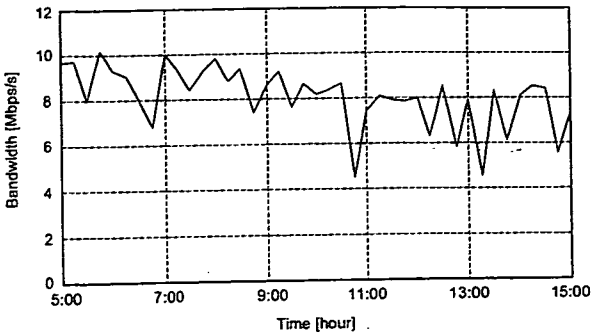

Fig.9 Time variation of the network bandwidth.

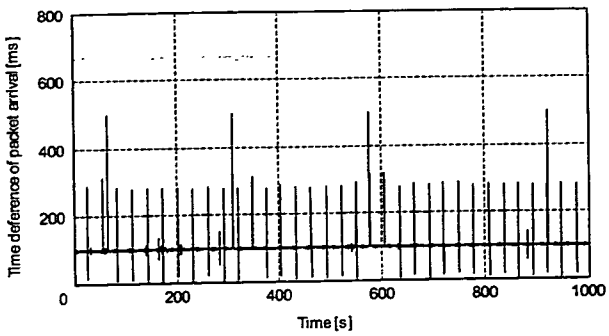

Fig.10 Time difference of packet arrival.

報伝送時間遅れ，スレーブ・マニピュレータの機械的応答速度，マスタ・スレーブ間の映像伝送時間遅れの総和によって得られる(**Table 6**)．これらは実用に足るとされる遠隔操作システムの要件を満たしている[11]．しかしながら，伝送時間遅れは操作感に大きく影響を与える要素であり，さらなる遅延の低減が望まれる．Marescauxらは，許容可能な遅延はおおよそ 330ms程度であると報告している[10]．この値は伝送時間遅れのみを考慮しており，送信周期，ロボットの機械的応答速度までを考慮した本研究での結果と単純に比較することは出来ない．本実験中，執刀医師は明らかに伝送遅延を認識しているものの，操作入力から映像が追従するのを待機するまでの遅延は生じなかったことが実験後の聞き取りにより確認された．

伝送時間遅れが操作性における大きな障害となる場合，フレームレートを低減する，またはMPEG 等を用いる場合において圧縮進展時間を考慮した上で伝送映像の圧縮率を上げる，等により伝送情報量を低減させ，伝送時間遅れを軽減することが可能となる．しかし一方で，伝送映像品質は手術を行なう上で重要な要素である．よって伝送する映像の系統数，品質は，伝送時間遅れとトレード・オフの関係にあり，使用帯域に適合した映像条件を選択することで，伝送時間遅れを減少させることが可能となる．

回線品質の変動：**Fig.9** にネットワーク帯域測定ツールiperf[9]を用い，両サイト間のロボット制御器を含むネットワーク・セグメント(上限 11Mbps)について，実験中の帯域を測定した結果を示す．本実験で用いたネットワーク環境においては，他のユーザの影響による回線品質の変動が予測されたが，実験中，午前 9 時以降に多少の帯域低下を生じたものの，大きな変動は観測されなかった．しかしながら，マスタからスレーブへの位置情報伝送において，スレーブでのデータ・パケット到着時間を測定したところ，動作には支障とならなかったものの，約 30s ごとに大きな遅れを生じていることが確認された(**Fig.10**)．この原因については，RIPによるルーティング，スパニングツリーの定期的動作等が考えられるが，本実験で行なったようなEnd-to-End での測定結果では明らかにできなかった．本実験では Hop Count が 14 と大きな値である．手術動作中，これらのルータを動作保証する手段，また回線品質の異常を検知するシステムの開発が必要と考えられる．手術のようなリアルタイム性を要するクリティカル・アプリケーションを大規模ネットワーク回線を介して利用する場合，回線品質の確保が重要となる．特に本実験で用いたような専用線以外の回線を使用する場合，QOS(Quality Of Service)制御等による回線品質確保が重要となる．

Table 6 Sensible time-delay of operator.

Network	Op. site – Surg. site	Time-delay
ISDN(2B+D)	Tokyo - Shizuoka	540.0 ms
ISDN(23B+D)	Tokyo - Shizuoka	592.5 ms
APII	Seoul - Fukuoka	592.5 ms

5. まとめ

日本－韓国を結ぶ学術研究用インターネットを使用し，低侵襲手術支援システムを用いた遠隔手術実験によって，ブタを対象とした腹腔鏡下胆嚢摘出術に成功した．本実験では，ロボット動作情報に加え，映像をDV 品質で 4 系統伝送した．伝送時間遅れはロボット動作情報伝送において 6.5ms, 映像伝送において 435msであった．本実験により，ロボットによる海外とを結ぶ遠隔手術が可能であることが確認された．しかしながら，伝送時間遅れは操作感に大きく影響を与える要素であり，さらなる遅延の低減が望まれる．伝送映像系統数，品質と伝送時間遅れはトレード・オフの関係

にあり，使用可能帯域に適合した映像条件を選択することで，伝送時間遅れの影響を軽減することが可能となる．遠隔手術において情報通信設備への要求は非常に高く，今後のさらなる整備が期待される．現状では，本実験で用いたような専用線以外の回線使用を使用する場合，QOS 制御等による回線品質確保に加え，通信経路の異常を検知するセーフティ・システム等が重要となる．

謝辞：本研究の一部は，東京大学 21 世紀COEプログラム「機械システム・イノベーション」，九州大学教育研究プログラム・研究拠点形成プロジェクト(P&P)「ロボット医学教育研究の戦略的拠点の形成」の支援のもと実施された．

文献

1) Gary S, Guthart J, K Salisbury Jr. The Intuitive Telesurgery System: Overview and Application. ICRA2000, San Francisco, 2000; 618-621.
2) Kumar R, Whitcomb L L, Taylor R H, et al. Preliminary Experiments in Cooperative Human/Robot Force Control for Robot Assisted Microsurgical Manipulation. ICRA2000, San Francisco, 2000; 610-617.
3) Ikuta K, Daifu S, Hasegawa T, Hashikawa H. Hyper-finger for Remote Minimally Invasive Surgery in Deep Area. MICCAI2002, Tokyo, 2002; 173-181.
4) 佐久間一郎．外科手術支援ロボティックシステムの開発．日本ロボット学会誌 2005; 23(5): 535-537.
5) Fujie M, Iseki H, Takakura K, et al. NeuRobot: telecontrolled micromanipulator system for minimally invasive microneurosurgery-preliminary results. Neurosurgery 2002; 51(4): 985-988.
6) Green P S, et al. Mobile Telepresence Surgery. MACAS'95, Baltimore, 1995; 97-103.
7) Arai F, et al. Multimedia Tele-surgery Using High Speed Optical Fiber Network and Its Application to Intravascular Neurosurgery. ICRA'96, Minneapolis, 1996; 878-883.
8) Rovetta A, et al. Robotics and Telerobotics Applied to a Prostatic Biopsy on a Human Patient. MRCAS'95, Baltimore, 1995; 104-110.
9) Salcudean S E, et al. Performance Measurement in Scaled Teleoperation for Microsurgery. CVRMed-MRCAS'97, Grenoble, 1997; 789-798.
10) Marescaux J, et al. Transatlantic robot-assisted telesurgery. NATURE 2001; 413: 379-380.
11) Kim W S, Bejczy A K. Demonstration of a High-Fidelity Predictive/Preview Display Technique for Telerobotic Servicing in Space. IEEE Trans. on Robotics and Automation 1993; 9(5): 698-702.
12) Sano A, Fujimoto H, Takai T. Network-Based Force-Reflecting Teleoperation. ICRA2000, San Francisco, 2000; 3126-3131.
13) Mitsuishi M, et al. Tele-micro-surgery system with intelligent user interface. ICRA2000, San Francisco, 2000; 1607-1614.
14) Mitsuishi M, Arata J, Hashizume M, et al. Development of a Remote Minimally-Invasive Surgical System with Operational Environment Transmission Capability. ICRA2003, Taipei, 2003; 2663-2670.
15) Arata J, Hashizume M, Mitsuishi M, et al. A remote surgery experiment between Japan-Korea using the minimally invasive surgical system. ICRA2006, Orlando, 2006; 257-262.
16) 田中勝弥，荒田純平，宮本学，割澤伸一，光石衛，堀健太，黒田知宏，小山博史．高速ネットワークを用いた遠隔微細手術システムにおける三次元視覚情報提示．日本機械学会ロボティクスメカトロニクス講演会 2003 予稿集 2003; 2P2-2F-C2.
17) APII, http://www-tc.tky.apii.net/
18) WIDE, http://www.wide.ad.jp/
19) iperf, http://dast.nlanr.net/Projects/Iperf/

J. Magn. Soc. Jpn., 31, 17–22 (2007) 〈Paper〉

High-Frequency Carrier-Type Magnetic Field Sensor with a Sub-pT Resolution Using a Magnetic Film and a Transmission Line

Y. Murayama, T. Ozawa[*1], S. Yabukami[**2], K. Ishiyama, and K.I. Arai[***3, ****4]
Research Institute of Electrical Communication, Tohoku Univ., *Katahira 2-1-1, Aoba-ku, Sendai 980-8577, Japan*

We developed a very sensitive high-frequency carrier-type magnetic field sensor with a sub-pT resolution using a resonating transmission line. Meander-type sensor elements using amorphous CoNbZr films were fabricated. We obtained a magnetic field resolution of 7.4 x 10^{-13} T/Hz$^{1/2}$ at 501 kHz. The detectable magnetic field was limited by the noise caused by nonlinear magnetic excitation. We analyzed the quality factor of the resonance for enhancement of the signal-to-noise ratio.

Key words: sub pT resolution, resonating transmission line, thin-film sensor, quality factor

10^{-13} T台の磁界検出分解能を有する高周波伝送線路型薄膜磁界センサ

村山芳隆・小澤哲也[*1]・藪上信[**2]・石山和志・荒井賢一[***3, ****4]
東北大学電気通信研究所，仙台市青葉区片平 2-1-1（〒980-8577）

1. はじめに

高透磁率磁性体へ高周波電流やパルス波を通電し，外部磁界を印加することで，その透磁率変化を介し，表皮効果及び自然共鳴によりインピーダンスが大きく変化することを利用した磁界センサは，GMI センサあるいは高周波キャリア型磁界センサと呼ばれ、高感度化の研究及び産業応用が議論されている[1)-5)]．この磁界センサの検出感度の限界は磁化の熱ゆらぎで決定されると考えられ，その値は室温で 10^{-13} T(7.95 x 10^{-8} A/m)台に達するとの報告がある[6)]．この磁界センサを高感度化するにはセンサ素子自体の感度を高めるとともに，信号検出時のノイズの抑制が重要である．

筆者らは，これまで磁性膜に直接高周波電流を通電させたタイプのセンサを開発してきた．磁性膜に直接通電するタイプの高周波キャリア型薄膜磁界センサではノイズレベルは主として位相雑音と熱雑音で決まることが報告されている[5)]．またセンサへの投入パワーを増加させることによる SN 比の悪化およびノイズレベルの上昇についての実験結果を報告した[7)]．

本稿ではキャリア電流を大きくした場合のノイズレベルの上昇を緩和することを意図し，磁性薄膜への直接通電を避ける構造のセンサ素子を検討した．センサ素子はキャリア電流を通電させる伝送線路と，近接配置した磁性薄膜から構成した．また共振を利用することでインピーダンス変化率を増大し，信号強度増大を図った．試作したセンサを用いて 501 kHz の交流磁界において 10^{-13} T (7.95 x 10^{-8} A/m) 台の磁界検出分解能を得た．

2. 伝送線路型薄膜磁界センサ

Fig. 1 は本論文で検討する磁界センサを模式的に示したものである．センサ素子はマイクロストリップ線路等の伝送線路の上部あるいは上下に磁性薄膜を近接配置した構造となっている．伝送線路と磁性薄膜の間はレジストで絶縁される．磁性薄膜の磁化容易軸は熱処理によって伝送線路の幅方向に付与する．バイアス磁界および交流磁界（測定磁界）は伝送線路の長手方向へ印加する．キャリア電流は伝送線路へ通電される．外部からの印加磁界によって磁性薄膜の磁化が回転し，透磁率が変化する．これにより伝送線路のインピーダンスが変化し，これを利用して交流磁界を検出する．以下本稿ではこの構造の磁界センサを伝送線路型センサと呼ぶ．

Fig. 2 は微小交流磁界の計測方法を概念的に示したものである．キャリア電流はシグナルジェネレータによりセンサ素子へ加えられ，出力信号はスペクトラムアナライザ等の 50Ω系の測定装置で計測される．センサ素子には，バイアス磁界をインピーダンス変化率が最大となるように印加している．スペクトラムアナライザで計測されるキャリア電流は交流磁界により振幅変調され，その側波帯は交流磁界の磁界強度に比例する．信号強度は線形領域での励振であれば，振幅変調波の側波帯[9)]として(1)式で近似できる．

$$\left|v_o(\omega_c \pm \omega_s)\right| = \frac{JS(Z_b+50)R_o h_{ac}}{2\{Z_b+R_o+R_i\}^2}\left(\frac{dZ}{dh}\right) \qquad (1)$$

ただし v_o は側波帯レベル，ω_c はキャリアの角周波数，ω_s

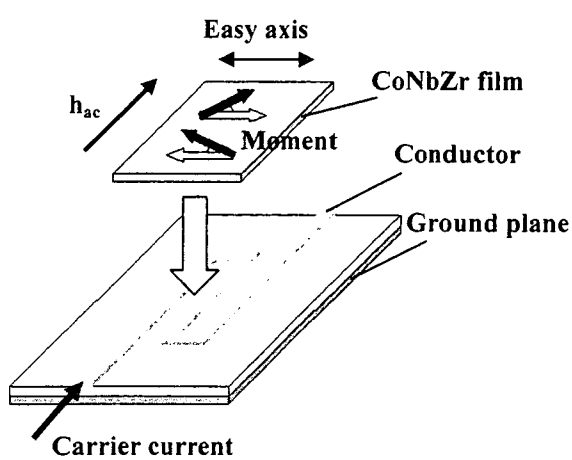

Fig. 1 Schematic view of the sensor element.

[*1] 宮城高等工業専門学校
[**2] 東北学院大学工学部
[***3] 電気磁気材料研究所
[****4] 情報通信研究機構

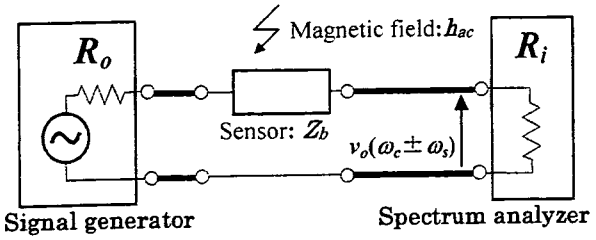

Fig. 2 Equivalent circuit.

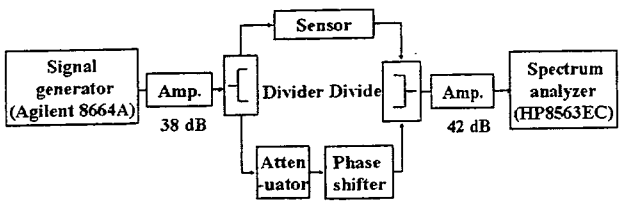

Fig. 3 Carrier-suppressing circuit.

は微小交流磁界の角周波数，J はセンサ素子に通電するキャリアの電流密度，S はセンサ素子の断面積，h_{ac} は測定される交流磁界強度，R_o はシグナルジェネレータの出力抵抗，R_i はスペクトラムアナライザの入力抵抗であり，Z_b は素子の動作点におけるインピーダンス，dZ/dh は印加磁界に対するインピーダンス変化率である．

3. 実験方法

3.1 センサ素子の作製

センサ素子はマイクロストリップ線路上にアモルファス $Co_{85}Nb_{12}Zr_3$ 薄膜を近接配置した構造となっている．マイクロストリップ線路は，厚さ 0.5 mm のテフロン基板（CHUCOH 製 CGK-500），あるいは厚さ 25 μm のポリイミド基板（SHIN-ETSU 製 RBF-1）をウェットエッチングによって作製した．$Co_{85}Nb_{12}Zr_3$ 薄膜は RF スパッタ法により投入電力は 200 W，Ar ガス圧は 20 mTorr の条件でガラス基板（MATSUNAMI 製 S-1111）に約 4 μm 成膜した．その後熱処理は回転磁界中熱処理（2 時間，3 kOe (238.5kA/m)，400℃）の後，静磁界中熱処理（1 時間，3 kOe (238.5kA/m)，150℃）を施した．$Co_{85}Nb_{12}Zr_3$ 薄膜の異方性磁界強度は 19.9 A/m (0.25 Oe)となった．熱処理後，磁性薄膜表面に絶縁層としてレジスト（ZEON 製 ZPN-1150）を約 5 μm 塗布した．作製したマイクロストリップ線路と磁性薄膜を重ね合わせて伝送線路型センサとした．磁性膜厚（約 4μm）および絶縁膜厚（約 5μm）は本論文の中で試作したセンサにおいては最も SN 比が高くなることから実験的に求めた．作製したセンサ素子のインピーダンスは，伝送線路長手方向に直流磁界をヘルムホルツコイルで印加しながら，ネットワークアナライザ（HP 8752A）を用いて透過法により測定した．

3.2 微小磁界計測

微小磁界計測には Fig. 3 に示す搬送波抑制回路（キャリアサプレス回路）[5] を用いた．シグナルジェネレータ（Agilent 8664A）から出力されるキャリアは，低雑音増幅器（NOGAWA NHP-2046）により増幅され，センサ側および減衰器側に分けられる．センサに印加される交流磁界はセンサ素子に通電されるキャリアにより振幅変調される．分岐されたもう一方ではキャリアを上段と振幅が等しく位相が 180° 異なるように，移相器（ARRA 2448A）および減衰器（Agilent 8494B，KEYCOM KAT-001010-M）により調整した．これらの信号を合成することでキャリア成分を 60 dB 以上抑制し，オフセット周波数 501 kHz における位相雑音を熱雑音以下に低減した．側波帯強度およびノイズレベルの測定はスペクトラムアナライザ（HP8563EC）を用いた．実験は全て，磁気シールドルーム（遮蔽率は 1 Hz で約 35dB，500 kHz で約 60 dB）で行った．

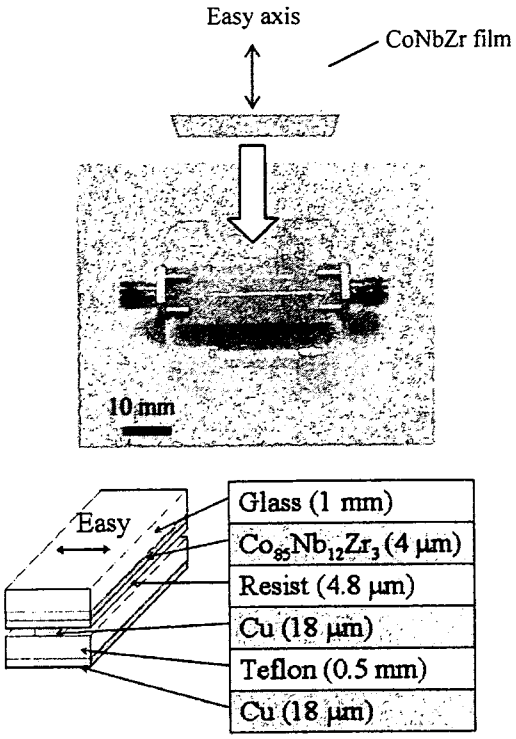

Fig. 4 Sensor element.

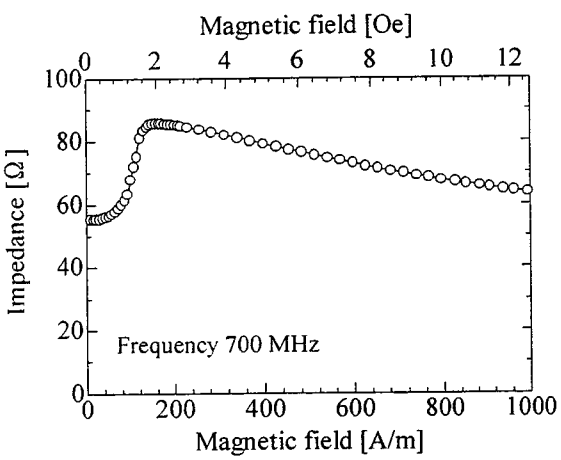

Fig. 5 Impedance of the sensor element.

4. 実験結果

4.1 直線状センサ素子

Fig. 4 に作製したセンサ素子の外観写真および断面の模式図を示す．伝送線路部分は厚さ 0.5 mm のテフロン基板